

Cell Biology  
Editor's Choice

## Inhibition of hyaluronan secretion by novel coumarin compounds and chitin synthesis inhibitors

Alexandra A Tsitrina<sup>1,†</sup>, Igor V Krasyllov<sup>2</sup>, Dmitry I Maltsev<sup>1</sup>,  
Irina N Andreichenko<sup>3</sup>, Viktoria S Moskvina<sup>2</sup>, Dmitry N Ivankov<sup>3</sup>,  
Elena V Bulgakova<sup>1</sup>, Mikhail Nesterchuk<sup>3</sup>, Vera Shashkovskaya<sup>3</sup>,  
Nataliya O Dashenkova<sup>1</sup>, Vladimir P Khilya<sup>2</sup>, Arsen Mikaelyan<sup>1</sup> and  
Yuri Kotelevtsev<sup>3,‡</sup>

<sup>1</sup>Laboratory of problems of regeneration, Koltzov Institute of Developmental Biology of Russian Academy of Sciences, 119334 Moscow, Russia, <sup>2</sup>Department of Organic Chemistry, Taras Shevchenko National University of Kyiv, 01601 Kyiv, Ukraine, and <sup>3</sup>Center for Neurobiology and Brain Restoration and Center of Life Sciences, Skolkovo Institute of Science and Technology, Skolkovo, 143025 Moscow, Russia

<sup>†</sup>To whom correspondence should be addressed: Yuri Kotelevtsev, Tel: +7-916-438-19-03; Fax: +7-495-280-14-82; e-mail: y.kotelevtsev@skoltech.ru. Alexandra A. Tsitrina, Tel: +7-962-905-89-87; Fax: +7-499-135-80-12; e-mail: sashulka.s@gmail.com

<sup>†</sup>Alexandra A. Tsitrina and Igor V. Krasyllov contributed equally and share the first authorship.

<sup>‡</sup>Yuri Kotelevtsev and Arsen Mikaelyan contributed equally and share the last authorship.

Received 8 February 2021; Revised 20 April 2021; Editorial Decision 20 April 2021; Accepted 20 April 2021

### Abstract

Elevated plasma levels of hyaluronic acid (HA) is a disease marker in liver pathology and other inflammatory disorders. Inhibition of HA synthesis with coumarin 4-methylumbelliferone (4MU) has a beneficial effect in animal models of fibrosis, inflammation, cancer and metabolic syndrome. 4MU is an active compound of approved choleric drug hycromone with low bioavailability and a broad spectrum of action. New, more specific and efficient inhibitors of hyaluronan synthases (HAS) are required. We have tested several newly synthesized coumarin compounds and commercial chitin synthesis inhibitors to inhibit HA production in cell culture assay. Coumarin derivative compound VII (10'-methyl-6'-phenyl-3'H-spiro[piperidine-4,2'-pyrano[3,2-g]chromene]-4',8'-dione) demonstrated inhibition of HA secretion by NIH3T3 cells with the half-maximal inhibitory concentration (IC<sub>50</sub>) = 1.69 ± 0.75 μM superior to 4MU (IC<sub>50</sub> = 8.68 ± 1.6 μM). Inhibitors of chitin synthesis, etoxazole, buprofezin, triflumuron, reduced HA deposition with IC<sub>50</sub> of 4.21 ± 3.82 μM, 1.24 ± 0.87 μM and 1.48 ± 1.44 μM, respectively. Etoxazole reduced HA production and prevented collagen fibre formation in the CCl<sub>4</sub> liver fibrosis model in mice similar to 4MU. Bioinformatics analysis revealed homology between chitin synthases and HAS enzymes, particularly in the pore-forming domain, containing the proposed site for etoxazole binding.

**Key words:** 4-methylumbelliferone, chitin synthase inhibitors, hyaluronic acid, hyaluronan synthase inhibitors, liver fibrosis

## Introduction

Recent experimental data reveal hyaluronan synthase 2 (HAS2) as an important drug target in fibrosis (Andreichenko et al. 2019; Yang et al. 2019), cancer (Sato et al. 2016) and metabolic syndrome (Grandoch et al. 2019). 4-methylumbelliferone (4MU) is the most widely used inhibitor of hyaluronan (HA) biosynthesis (Nagy et al. 2015). Several other compounds were reported to inhibit HA secretion by different cell lines, including analogues of nonsteroid estradiol receptor agonists (Mason et al. 1984) multidrug resistance inhibitors, valsopodar or verapamil (Prehm and Schumacher 2004), vesnarinone (Ueki et al. 2000), fluoxetine (Prozac) amitriptyline (Yaron et al. 1999) and some other reviewed in (Kudo et al. 2017). None of those compounds was shown to be direct inhibitors of HAS, and different mechanisms of action were proposed. Characterization of inhibitors of HA production directly interacting with HAS is essential for the perspective drug development.

4MU is a natural coumarin compound of plant origin. It is used for cholestasis treatment under the trade name “Hymecromone.” The inhibitory effect of 4MU on HA production by human fibroblasts in culture was first discovered in 1995 (Nakamura et al. 1995) by chance during the investigation of  $\beta$ -xyloside induction of galactosaminoglycan synthesis. It was shown that not only  $\beta$ -xyloside-4MU but also 4MU itself inhibited the production of HA in human fibroblasts. Simultaneously, 4MU did not affect the synthesis of other glycosaminoglycans (chondroitin 4-sulfate, chondroitin 6-sulfate and dermatan sulfate) in concentrations of up to 1 mM. In the cell-free assay using plasma membrane preparations containing hyaluronan synthase activity (Mian 1986) 4MU did not inhibit HA synthesis (Nakamura et al. 1997). 4MU is a substrate for UDP-glucuronyltransferases. It was suggested that exhaustion of the availability of HAS substrate UDP-GlcUA in the presence of 4MU might partially account for the inhibition of HA synthesis in mammalian cells (Kakizaki et al. 2004). Incubation with 4MU depleted UDP-GlcUA levels by 38–95% in A2058 melanoma cells, MCF-7 and MDA-MB-361 breast, SKOV-3 ovarian and UT-SCC118 squamous carcinoma cells (Kultti et al. 2009). It is well accepted that 4MU may have a complex effect on HA production. Substrate depletion (Kakizaki et al. 2002) is considered to be one of the possible reasons for the 4MU inhibitory effect on HA production. However, other mechanisms may also be fundamental, particularly at the lower concentration range.

4MU may regulate HA production on a transcriptional level. Kakizaki and others demonstrated downregulation of HAS2 gene expression by 4MU (Kakizaki et al. 2004; Kultti et al. 2009; Vigetti et al. 2009; Saito et al. 2013; Sukowati et al. 2019). HAS2 expression must be regulated by nuclear receptors, particularly by glucocorticoid receptors. The expression of HAS2 mRNA is suppressed by dexamethasone (Zhang et al. 2000). Glucocorticoids induce fast and prolonged, near-complete suppression of HAS2 mRNA levels, mediated through decreases in both transcription rates and the message half-life (Zhang et al. 2000).

The Hirasaki University group first undertook the structural-functional analysis of 4MU derivatives in relation to HA synthesis. Several compounds with substitution of methyl and hydroxyl groups were investigated on the ability to inhibit HA production in cell lines at a fixed nontoxic concentration of 10  $\mu$ M. Both methyl groups and hydroxyl groups were essential for inhibitory activity. In compounds retaining the 4-methyl group, inhibitory activity decreased in a row 4MU > 6,7-dihydroxy-4-methyl coumarin > 5,7-dihydroxy-

4-methyl coumarin > umbelliferone and finally, 7-methoxy-4-methyl coumarin (incapable of making glucuronide compounds) were inactive at concentration 10  $\mu$ M (Morohashi et al. 2006). We have synthesized several analogues of 4MU, intending to investigate the structure-functional relationship in cell culture hyaluronan production assays.

Mammalian HAS1, HAS2 and HAS3, belong to class I hyaluronan synthases (HAS) with chain elongation from the reducing end (Weigel 2015). They share homology, and with the protein encoded by DG42 (Spicer and McDonald 1998), a gene differentially expressed during the embryonal development of *Xenopus* (Sargent and Dawid 1983). The latter shared homology with yeast chitin synthase and was able to synthesize chitin in vitro and in vivo (Semino and Robbins 1995). Soon it was shown that DG42 is a hyaluronan synthase in vivo (Meyer and Kreil 1996; Varki 1996). Mammalian HAS indeed possess chitin synthase activity, which was carefully investigated by Weigel (2015) and Weigel et al. (2017). It was found that HAS, plant cellulose synthases and chitin synthases (CHS) comprise a family with functional and structural similarities, which are reflected in domain structures. The template enzyme shares a high functional similarity and a low sequence similarity (~15%) with bacterial SeHAS. Despite the poor sequence similarity, modelled 3D structures of HAS domains were of high quality as indicated by the global ( $P$ -value: 10<sup>-8</sup>) and absolute (GDT score: 5–2) quality measurements (Agarwal et al. 2019).

It prompted us to hypothesize that some chitin synthesis inhibitors may also inhibit hyaluronan production.

## Results

### Estimation of cell toxicity

Coumarin derivatives and chitin synthesis inhibitors used in this study are listed in Figure 1.

To measure the inhibitory effect of listed compounds on hyaluronan secretion, we first evaluated their potential toxicity. MTT cell viability assay was performed on proliferating NIH3T3 cells (mouse fibroblast cell line) after 3 days of incubation with rising concentrations of different inhibitors (Figure 2A).

Compounds I–IV, VI and IX were not toxic in concentrations up to 0.5 mM and did not affect cell viability at concentrations up to 1 mM. Compounds V, VII and VIII demonstrated toxicity at concentrations higher than 125, 30 and 60  $\mu$ M, correspondingly. Chitin inhibitors did not possess any toxic effect in the tested concentrations.

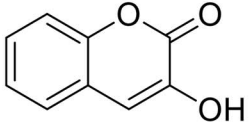
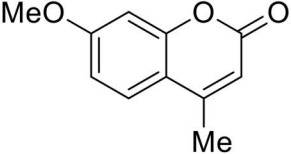
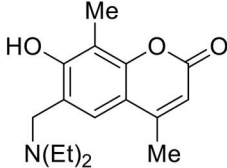
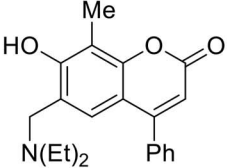
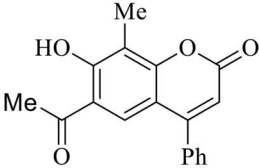
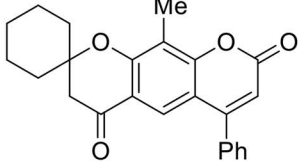
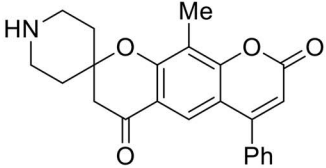
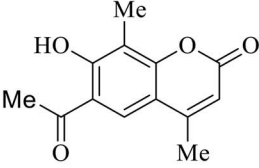
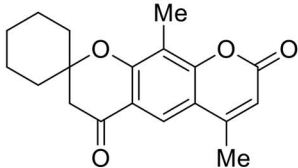
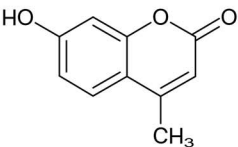
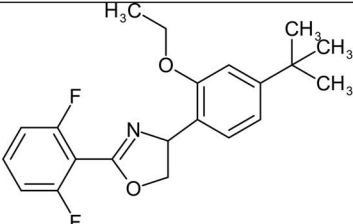
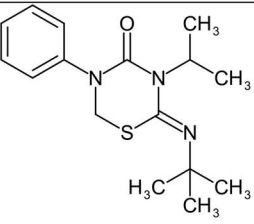
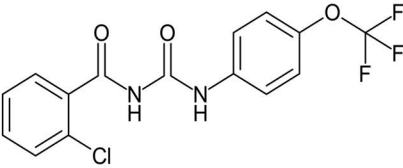
We also estimated the effect of tested compounds on cell population doubling time (Figure 2B).

As expected, 4MU increased doubling time gradually in the concentration range from 60  $\mu$ M to 1 mM. At 250  $\mu$ M of 4MU, doubling time increased is nearly twice (from 21 h till 38 h).

Compounds I–VI did not affect cell population doubling time. Compounds V and IV increased it gradually from concentrations 125 and 500  $\mu$ M, respectively.

Compounds VII and VIII increased the doubling time at concentrations over 10 and 50  $\mu$ M, respectively. Compound IX slightly speeded up the cell cycle and decreased doubling time from 21 to 16.5 h at all tested concentrations.

The chitin inhibitors did not affect cell viability at concentrations up to 1 mM. All of them decreased the doubling time from 21 to 17 h at all tested concentrations.

4MU derivatives		
		
I. Molecular Weight: 162.14	II. Molecular Weight: 190.20	III. Molecular Weight: 275.34
		
IV. Molecular weight: 337.41	V. Molecular Weight: 294.30	VI. Molecular Weight: 374.43
		
VII. Molecular Weight: 375.42	VIII. Molecular Weight: 232.23	IX. Molecular Weight: 312.36
4-methylumbelliferone		
		
Molecular Weight 176.17		
Chitin synthase inhibitors		
		
Etozazole (Eto) Molecular Weight: 359.417	Buprofezin (Bup) Molecular Weight: 305.44	Triflumuron (Trif) Molecular Weight: 358.70

**Fig. 1.** List of tested coumarin derivatives and chitin synthesis inhibitors: 2-hydroxy coumarin (I); 7-methoxy-4-methyl coumarin (II); 6-((diethylamino)methyl)-7-hydroxy-4,8-dimethyl-2H-chromen-2-one (III); 6-((diethylamino)methyl)-7-hydroxy-8-methyl-4-phenyl-2H-chromen-2-one (IV); 6-acetyl-7-hydroxy-8-methyl-4-phenyl-2H-chromen-2-one (V); 10'-methyl-6'-phenyl-3'H-spiro[cyclohexane-1,2'-pyrano[3,2-g]chromene]-4',8'-dione (VI); 10'-methyl-6'-phenyl-3'H-spiro[piperidine-4,2'-pyrano[3,2-g]chromene]-4',8'-dione (VII); 6-acetyl-7-hydroxy-4,8-dimethyl-2H-chromen-2-one (VIII); 6',10'-dimethyl-3'H-spiro[cyclohexane-1,2'-pyrano[3,2-g]chromene]-4',8'-dione (IX); 7-hydroxy-4-methylchromen-2-one (4MU); 4-(4-tert-butyl-2-ethoxyphenyl)-2-(2,6-difluorophenyl)-4,5-dihydro-1,3-oxazole (etozazole); 2-(tert-butylimino)-5-phenyl-3-(propan-2-yl)-1,3,5-thiadiazinan-4-one (buprofezin); 2-chloro-N-[[4-(trifluoromethoxy) phenyl]carbamoyl] benzamide (triflumuron). This figure is available in black and white print and in color at *Glycobiology* online.

### Inhibition of hyaluronan secretion by NIH3T3 fibroblast cell culture by coumarin compounds and chitin synthesis inhibitors

Inhibitory activity on hyaluronan accumulation in cell culture media by coumarin derivatives and chitin synthesis inhibitors in NIH3T3 cells are shown in [Figure 3](#) and calculated  $IC_{50}$  values presented in [Table I](#). Of note, for the compounds showing toxicity in the MTT test

(V, VII and VIII), the  $IC_{50}$  values were significantly below the toxicity range.

As it was reported by [Morohashi et al. \(2006\)](#), methylation of 7-hydroxy group of 4MU (7-methoxy-4-methyl-coumarin, compound II) abrogated its inhibitory activity almost completely with  $IC_{50}$  increased from  $8.68 \pm 1.6 \mu\text{M}$  (4MU) to  $223 \pm 140 \mu\text{M}$  supporting an essential role of the free 7-hydroxy group

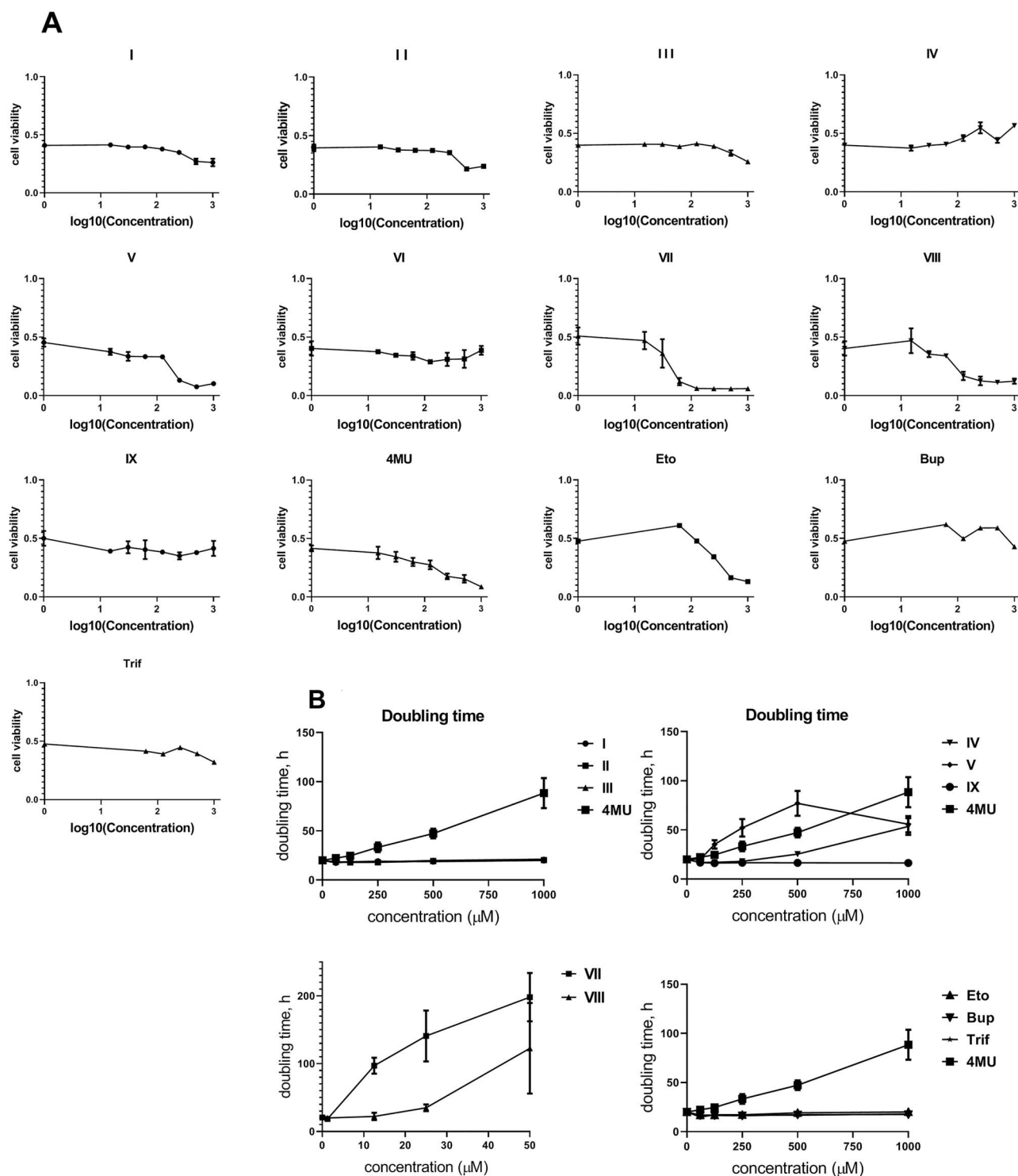


**Fig. 2.** (A) MTT assay cytotoxicity curves for compounds I-IX, Eto, Bup, and Trif. (Data present as mean  $\pm$  SD, cell viability is present in log scale),  $n = 3$ . (B) cells doubling time (Data present as mean  $\pm$  SD),  $n = 3$ . This figure is available in black and white in print and in color at *Glycobiology* online.

for HAS inhibitory activity. Compounds containing a 7-hydroxy group but bearing a positively charged diethylamino group in position 6 (compounds III and IV) had  $IC_{50}$  10 times higher than 4MU (Figure 3A). Interestingly, the substitution of a methyl group (III) for phenyl (IV) had almost no effect on the  $IC_{50}$  of these two compounds. The neutral acetyl group in position 6

only moderately reduced  $IC_{50}$  compared with 4MU in compound V ( $42.52 \pm 21.28 \mu\text{M}$ ) and VIII ( $17.74 \pm 10.55 \mu\text{M}$ ), with the last (6-acetyl-7-hydroxy-4,8-dimethyl-2H-chromen-2-one) slightly more active than 6-phenyl derivative (V). Spiropyranocumarines (VI and IX) derived from compounds V and VIII by reaction with cyclohexanone and simultaneous conversion of 7-hydroxyl to ether

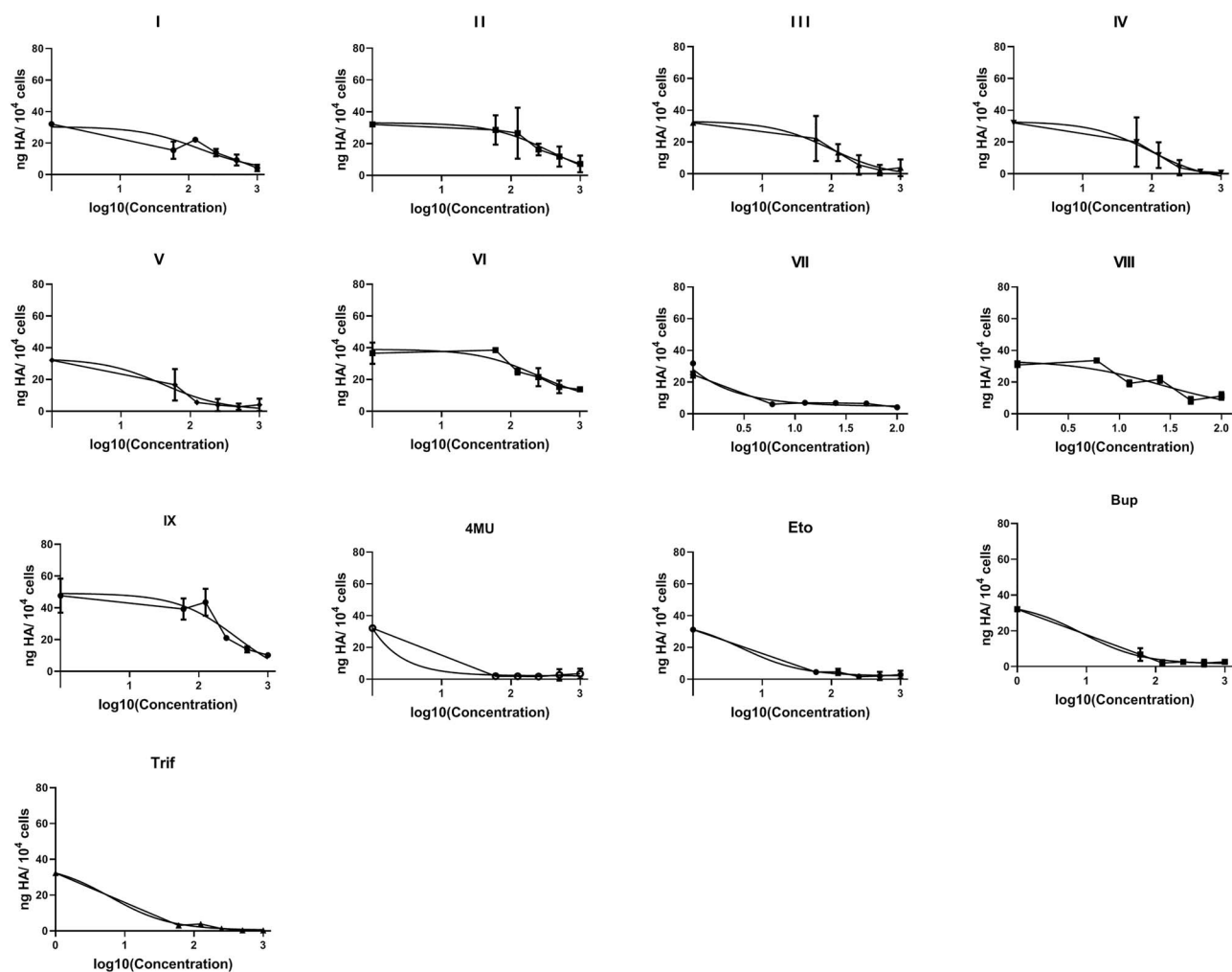


**Fig. 3.** Inhibition of HA deposition in the cell culture media of NIH3T3 cells treated by different concentrations of coumarin compounds and chitin synthesis inhibitors; data present mean  $\pm$  SD,  $n=3$ . This figure is available in black and white in print and in color at *Glycobiology* online.

**Table I.** The  $IC_{50}$  for inhibition of hyaluronan deposition in cell culture media by coumarin compounds and chitin synthesis inhibitors

Compound	$IC_{50}$ (Mean $\pm$ SD)	Compound	$IC_{50}$ (Mean $\pm$ SD)
I	145.6 $\pm$ 92.4 $\mu$ M	VIII	17.74 $\pm$ 10.55 $\mu$ M
II	223.1 $\pm$ 140 $\mu$ M	IX	362.5 $\pm$ 154.6 $\mu$ M
III	100.3 $\pm$ 61.98 $\mu$ M	4MU	8.68 $\pm$ 1.6 $\mu$ M
IV	100 $\pm$ 65.88 $\mu$ M	Eto	4.21 $\pm$ 3.82 $\mu$ M
V	42.52 $\pm$ 21.28 $\mu$ M	Bup	1.24 $\pm$ 0.87 $\mu$ M
VI	250 $\pm$ 164.4 $\mu$ M	Trif	1.48 $\pm$ 1.44 $\mu$ M
VII	1.69 $\pm$ 0.75 $\mu$ M		

Data present as mean  $\pm$  SD,  $n=3$ .

oxygen completely abrogated inhibition of hyaluronan production by NIH3T3 cells with  $IC_{50}$  almost an order of magnitude higher than of 4MU. Coumarin derivative compound VII (10'-methyl-6'-phenyl-3'H-spiro[piperidine-4,2'-pyrano[3,2-g]chromene]-4',8'-dione) demonstrated inhibition of HA secretion by NIH3T3 cells with the half-maximal inhibitory concentration ( $IC_{50}$ ) = 1.69  $\pm$  0.75  $\mu$ M superior to 4MU ( $IC_{50}$  = 8.68  $\pm$  1.6  $\mu$ M; **Figure 3** and **Table I**).

All tested chitin synthesis inhibitors were nontoxic at concentrations up to 1 mM. Etoazole and buprofezin had  $IC_{50}$  for inhibition of hyaluronan deposition in the low micromolar range (4.21  $\pm$  3.82  $\mu$ M and 1.24  $\pm$  0.87  $\mu$ M, correspondingly; **Table I**).

Triflumuron—a close analogue of Lufenuron—also inhibited the deposition of HA ( $IC_{50}$  = 1.48  $\pm$  1.44  $\mu$ M).

Calculated  $IC_{50}$  for 4MU, compounds of VII, VIII and chitin synthesis inhibitors determined by HBP ELISA protocol appeared in the low micromolar range. For testing the effect of these inhibitors on cells associated with HA, we treated cells with five different inhibitors in concentration 10  $\mu$ M for 3 days. We stained them with hyaluronan binding protein (HABP)—a specific probe for HA. Dimethyl sulfoxide (DMSO; 0.05% volume) was used as a positive control, and hyaluronidase digestion of untreated cells served as a negative control (**Figure 4 A** and **B**). In positive control cells, HA forms tangled fibers on the cell surface in areas of a high-density (**Figure 4A**, arrow). Treatment with 10  $\mu$ M of 4MU, compound VII, VIII and chitin synthesis inhibitors decreases the percentage of HA-positive area at least 3 times (**Figure 4B**), while hyaluronidase treatment obliterated HBP staining. HA fibers were rare or absent after treatment with inhibitors. A few numbers of HBP positive structures still present were thinner and shorter compared with positive control.

## Etoazole and 4MU affected expression levels of HAS2, HAS3 and Hyal1/2 at concentrations 2 orders of magnitude higher than their IC<sub>50</sub> determined in HA secretion assay

It is well known that 4MU inhibits HAS2 expression *in vivo* and *in vitro* (Nagy et al. 2015).

To investigate transcriptional effects of 4MU and etoazole on crucial enzymes of HA metabolism in the NIH3T3 cell line, we measured the expression levels of HAS2 and HAS3. HAS1 was undetectable in NIH3T3 cells with MEF cell line used as a positive control (Supplementary Figure 1).

4MU significantly inhibited HAS2 expression and upregulated Hyal1 expression with IC<sub>50</sub> ~250  $\mu$ M and activated HAS3 expression at concentration over 500  $\mu$ M (Figure 5). Hyal2 expression was not affected by 4MU at concentrations up to 1 mM. Etoazole at concentration 120- $\mu$ M upregulated HAS2 expression nearly 1.5 times, but higher doses suppressed it up to 80%. It also inhibited HAS3 expression at concentrations higher than 250  $\mu$ M. Hyal1 level significantly dropped at all tested concentrations, whereas the level of Hyal2 was not affected.

## Etoazole ameliorates CCl<sub>4</sub> induced liver fibrosis in mice

Next, we tested the effect of etoazole in the mouse model of CCl<sub>4</sub>-induced liver fibrosis.

Measurement of aspartate aminotransferase (AST) and alanine aminotransferase (ALT) levels in experimental animals' blood demonstrated that 4MU or etoazole did not prevent initial hepatocyte damage induced by toxic derivatives of CCl<sub>4</sub>. Etoazole and 4MU alone showed no hepatotoxicity at a daily dose of 600 mg/kg (Figure 6).

Fibrosis development was accompanied by a nearly 4-fold increase in HA blood concentration in CCl<sub>4</sub>-treated mice. Notably, both etoazole and 4MU (at 600-mg/kg daily) reduced plasma HA to near the control levels (Figure 6).

Previously, we have shown (Andreichenko et al. 2019) that genes involved in hepatocyte lipid metabolism were downregulated by CCl<sub>4</sub> and upregulated by CCl<sub>4</sub>/4MU treatment. This prompted us to check cholesterol and triglycerides levels in the blood of treated mice. Triglycerides level was not affected in CCl<sub>4</sub>, or CCl<sub>4</sub>/inhibitors treated groups. The cholesterol level was elevated in CCl<sub>4</sub>-treated animals.

We did not find any significant differences between the control group and groups of mice treated by only 4MU and Etoazole (Figure 6).

Next, we evaluated the influence of etoazole and 4MU on collagen deposition and fibrotic scar formation. As we have previously shown (Andreichenko et al. 2019), 4MU treatment prevented collagen deposition in the liver of CCl<sub>4</sub> treated animals. We did not observe extracellular fibrous collagen in CCl<sub>4</sub>/Eto. Instead, we found clumps of cells located at fibrous scars formation with increased affinity to aniline blue, which usually stains collagen, cartilage matrix and mucus in blue color. A small number of such cells can be found in place of current scar formation in CCl<sub>4</sub>-treated animals (Figure 7A).

Western blot analysis revealed a significant reduction of  $\alpha$ SMA level in CCl<sub>4</sub>/Eto-treated samples (Figure 7B).

Hepatic stellate cells (HSCs) and macrophages are two main cell types that drive fibrosis development. After tissue damage, HSCs transdifferentiate to myofibroblasts and, together with macrophages,

tend to migrate to the sites of injury. For estimation of the distribution of these cells in the liver parenchyma, we performed immunochemical staining for desmin—a marker of activated HSCs (Niki et al. 1999; Puche et al. 2013) and CLEC4F/CLECSF13—a marker of Kupffer Cells (KCs; Guillot et al. 2020), the resident macrophages. Confocal microscopy and quantitative image analysis showed that only 6% of desmin positive cells were found near 15% of CLEC4F/CLECSF13 positive KCs in control samples. After CCl<sub>4</sub> treatment, partial representation of both cell types found close in the scar area was increased significantly (30% HSCs and 27% of KCs). Treatment with etoazole or 4MU decreases the association of HSCs and KCs (Figure 8 and Table II) in the scar area, which is reflected by a reduction of both MCC coefficients.

## Protein structure analysis of chitin synthase and hyaluronan synthase suggests the binding site of etoazole on the MD5 pore-forming domain

Etoazole was shown previously to inhibit chitin synthesis in mites. Genetic evidence supports the hypothesis that this and some other insecticides inhibit chitin deposition through binding to specific amino acid residues of chitin synthase. Point mutation I1017F makes spider mites completely resistant to etoazole (Douris et al. 2016). The introduction of this mutation to *Drosophila* also produces resistance to etoazole, benzoylurea insecticides and buprofezin. This supports the hypothesis that etoazole inhibits chitin synthase in mites through binding to alpha-helix in the 5TMS domain of chitin synthase containing Ile-1017 (Douris et al. 2016). We hypothesized that the corresponding site in HAS might be a target site for etoazole (Figure 9).

Using UniProt and NCBI databases, we performed a bioinformatics analysis to align protein sequences and domain structures of hyaluronan synthase 2 (HAS2) and insect CHS from different species. The Mouse and Human HAS and *Plutella xylostella* and *Drosophila melanogaster* CHS protein sequences were aligned.

We constructed a schematic topological model that showed high structural similarities between CHS and HAS molecules (Figure 9B). The protein alignment analysis showed that the HAS and CHS catalytic domains contained a conserved sequence motif Q\*\*RW (position 893–897 a.a. for CHS and 380–384 a.a. for HAS2). The C-terminal transmembrane domain included the WGT\* conserved sequence motif (position 463–466 a.a. for HAS2 and 1062–1065 a.a. for CHS).

We have identified Leu-447 in HAS2 amino acid sequences that correspond to Ile-1017 in the 5TMS domain of chitin synthase (Figure 9B and C).

Therefore, we have found significant homology both in primary amino acid sequence and in domain organization which supports our hypothesis that chitin synthesis inhibitors may inhibit hyaluronan production via direct interaction with HAS enzyme. Predicted 3D structure of HAS2 obtained with I-TASSER protein structure (Yang and Zhang 2015) and functional prediction server is shown in Figure 9A, with MD5 domain bearing Leu-447 homologous to alpha-helix of 5TMS domain bearing Ile-1017 colored in red.

## Discussion

Published data strongly support the development of the specific inhibitors of hyaluronan production for therapeutic application. The only available now compound 4-MU has low bioavailability and manifests effects *in vivo* in relatively high concentrations.

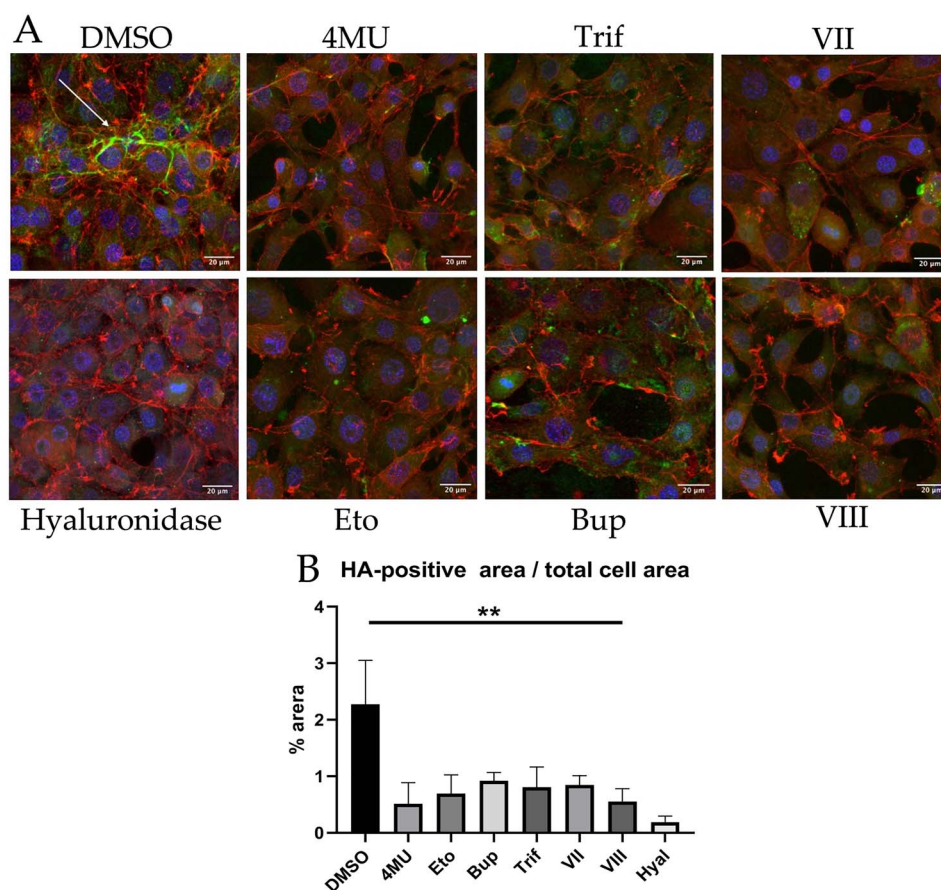


**Fig. 4.** Quantitative immunofluorescence analysis of hyaluronan associated with NIH3T3 cells after treatment with coumarin compounds and chitin synthesis inhibitors. **(A)** Fluorescent HABP staining after 72-h growth in the presence of inhibitors (10  $\mu$ M). Hyaluronic acid in Green; F-actin in Red; DNA in Blue; arrow—HA threads). Scale bar—20  $\mu$ m **(B)** Relative hyaluronan positive area in per cent to the total cell area. Data present as mean  $\pm$  SD,  $n = 3$ ; \*\*— $P < 0.01$  compared with control. Hyaluronidase treated cell (1 mg/mL in PBS, 30 min +37°C) was used as a negative control. This figure is available in black and white in print and in color at *Glycobiology* online.

Here, we present the dose-effect curve for 4MU inhibition of HA deposition in cell culture at a low micromolar range. Calculated  $IC_{50}$  for 4MU was as low as  $8.68 \pm 1.6 \mu$ M. This is much lower than the commonly used dose of 4MU in cell culture or in-vivo experiments. However, our data are in good correspondence with the low micromolar effects of 4MU published earlier (Prehm 2005, 2013, Morohashi et al. 2006). Also, 30% reduction of hyaluronan secretion by endothelial cells in the presence of as low as 0.6  $\mu$ M of 4MU was reported (Nagy et al. 2010). The same group published HA production inhibition in B16F10 cells by 50% in the presence of 30  $\mu$ M of 4MU (Nagy et al. 2019). Moreover, the effective plasma concentration of 4MU in mice fed with 5% chow averaged at only  $0.89 \pm 0.51 \mu$ g/mL or  $5.1 \pm 2.9 \mu$ M over 24 h (Kuipers et al. 2016).

4-MU is a relatively small molecule and does not allow extensive chemical modification. Removing of the 4-methyl group and particularly esterification of the 7-hydroxy group dramatically reduce its inhibitory activity. We report results on testing nine umbelliferon derivatives and three chitin synthase inhibitors for their ability to inhibit extracellular deposition of HA by NIH3T3 mouse fibroblast cell line. Our data support previous findings showing that the free 7-hydroxy group of 4-MU is essential, and its methylation almost wholly abolishes the inhibitory activity of 4-MU. Bulky neutral substitutions in position 6 reduce the activity, and the addition of a positive charge in position 6 reduces it even further (III and IV).

Surprisingly, compound VII, although lacking a free hydroxyl group in the seventh position with oxygen atom included in the pyranose ring, possessed strong HA synthesis inhibitory activity in the micromolar range, below its toxicity level. Of note, this compound was somewhat toxic; however, its toxicity was manifested at concentrations over 50  $\mu$ M. Compound VII lacks a free hydroxyl in position 7 and hence cannot be a substrate for UDP glycosylation. Therefore, its inhibitory activity cannot be explained by depleting the UDP-GlcUA substrate as a mechanism of inhibitory action by 4-MU (Kultti et al. 2009).

In this paper, we demonstrate for the first time that chitin synthesis inhibitors, etoxazole, buprofezin and triflumuron in low  $\mu$ M concentration range reduce HA secretion by NIH3T3 fibroblasts. All of them were nontoxic in the tested concentration range from 1  $\mu$ M to 1 mM.

These data corroborate the previous finding demonstrating that HA polymer synthesis starts with the assembly of chitin oligosaccharide primers by class I HAS enzymes (Weigel et al. 2015, 2017). Cellulose, chitin and hyaluronan are the three most abundant linear carbohydrate polymers on Earth (Spicer and McDonald 1998). Structural relation of cellulose synthase, chitin synthase and HAS was first recognized more than 25 years ago. Mammalian HAS belong to class I HAS, the transmembrane proteins (Rosa et al. 1988; DeAngelis et al. 1994; Pummill et al. 1998), which share several amino acid signatures

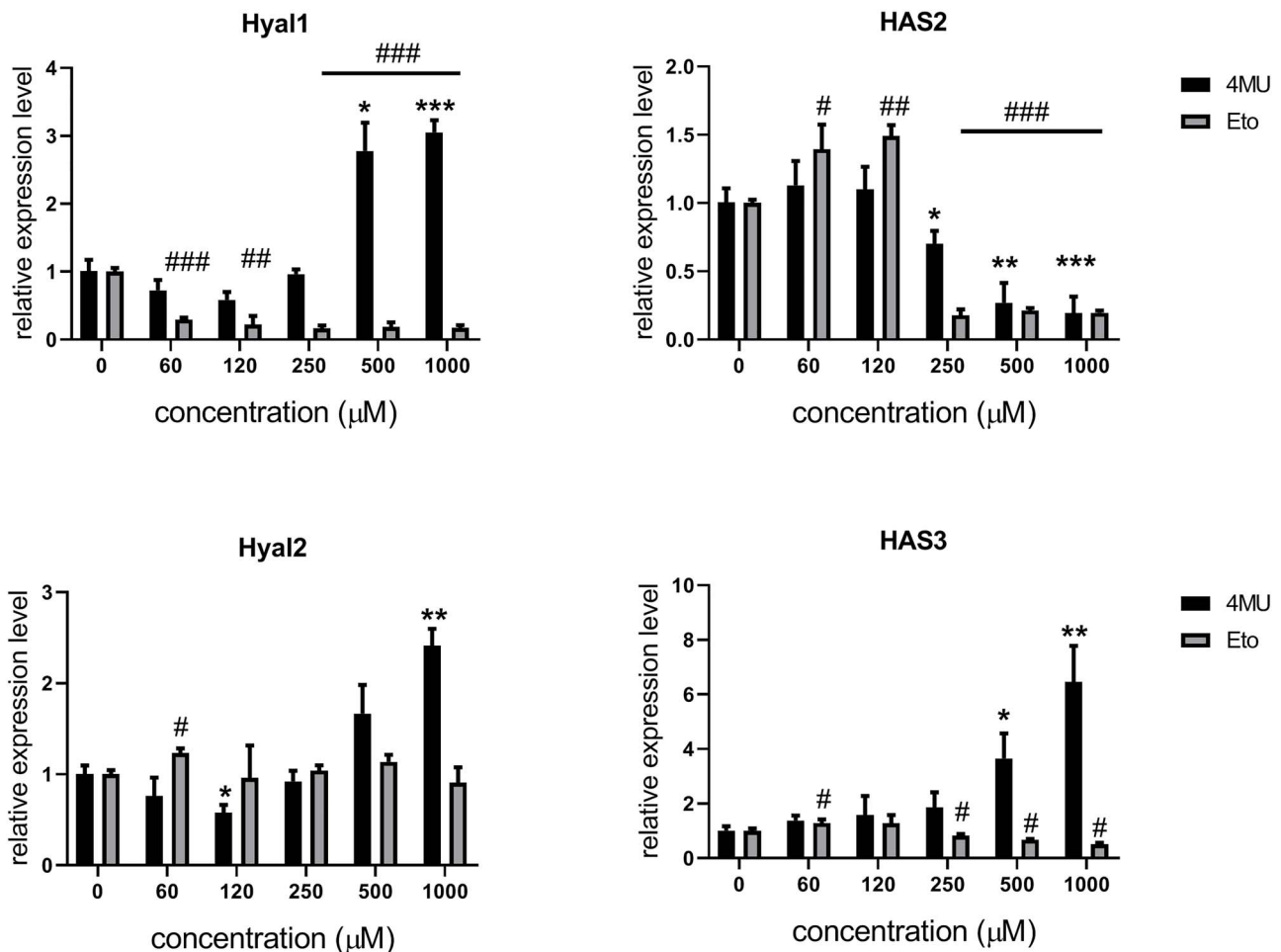


**Fig. 5.** Effect of etoxazole and 4MU on HAS2, HAS3 and Hyal1 and Hyal2 relative expression in NIH3T3 cells. Data present as mean  $\pm$  SD,  $n = 3$ , \*\*\*— $P < 0.001$  (one-way ANOVA). This figure is available in black and white in print and in color at *Glycobiology* online.

(QRRRW, CATMWHXT, QXFEY and WGTRE) with chitin synthase (Merzendorfer and Zimoch 2003), cellulose synthases (Saxena et al. 2001) and *N*-actetylglucosaminyltransferases such as the NodC protein (Geremia et al. 1994). These enzymes share common domains and are organized in the plasma membrane in a similar way (Agarwal et al. 2019). It was proposed that HAS are evolutionary related to CHS (Stern 2017).

UDP-GlcNAc is a common substrate for both CHS and HAS. This prompted us to suggest that substrate analogues of insect and fungal CHS peptidyl nucleoside antibiotics, such as polyoxins and nikkomyocins, will be able to inhibit HAS activity. However, nikkomyocin was ineffective in our NIH3T3 HA production assay (results not shown), which may be due to its known low permeability (Merzendorfer 2006). On the contrary, oxazoline and benzoylurea insecticides demonstrated potent inhibitory activity (Table I). These effective commercial insecticides interfering with chitin synthesis on larva and nymph stage have been in use for decades (Cohen 2001); however, their molecular mechanism of action was discovered only in the post-genome era.

Natural mutant strains of *Tetranychus urticae* (the two-spotted spider mite) resistant to etoxazole were used to produce segregating crosses. Using a combination of complementation tests, linkage analysis and new generation sequencing, a nonsynonymous mutation

I1017F was identified within the last transmembrane helix of the predicted C-terminal 5 transmembrane segment (5TMS) of chitin synthase (Van Leeuwen et al. 2012). This region is far away from the catalytic site but has been suggested to be involved in pore formation and chitin extrusion. Amino acids of 5TMS form a transmembrane helix with the sequence either identical or similar between insect/mite CHS1 and yeast CHS3. Intriguingly, the highly conserved arthropods and insects' isoleucine-1017 is immediately followed by a universally conserved proline, an amino acid usually involved in  $\alpha$ -helix breaking and formation of molecular hinges important for integral membrane protein function (Cordes et al. 2002). Resistance to clofentezine and hexythiazox, acaricides of different chemical structures, was also linked with the same I1017F mutation in *T. urticae* (Demaeght et al. 2014). It was suggested that other chitin synthesis inhibitors such as the benzoylphenyl urea (BPU), diflubenzuron also target extrusion pore. BPU compounds inhibit chitin synthesis in cell-intact systems only, but they are ineffective in membrane preparations which leads to the suggestion that they act on a postcatalytic step, i.e. pore extrusion (Merzendorfer 2006; Demaeght et al. 2014). *Drosophila* line resistant to diflubenzuron (LC<sub>50</sub> WT, 0.322 mg/L vs. LC<sub>50</sub> mutEt15, > 5000 mg/L), buprofezin (LC<sub>50</sub> WT, 53.2 mg/L vs. LC<sub>50</sub> mutEt15, > 1000 mg/L and lufenuron (LC<sub>50</sub> WT 0.148 mg/L vs. LC<sub>50</sub> Et15, 16.659 mg/L) was generated by CRISPR/Cas9 mediated



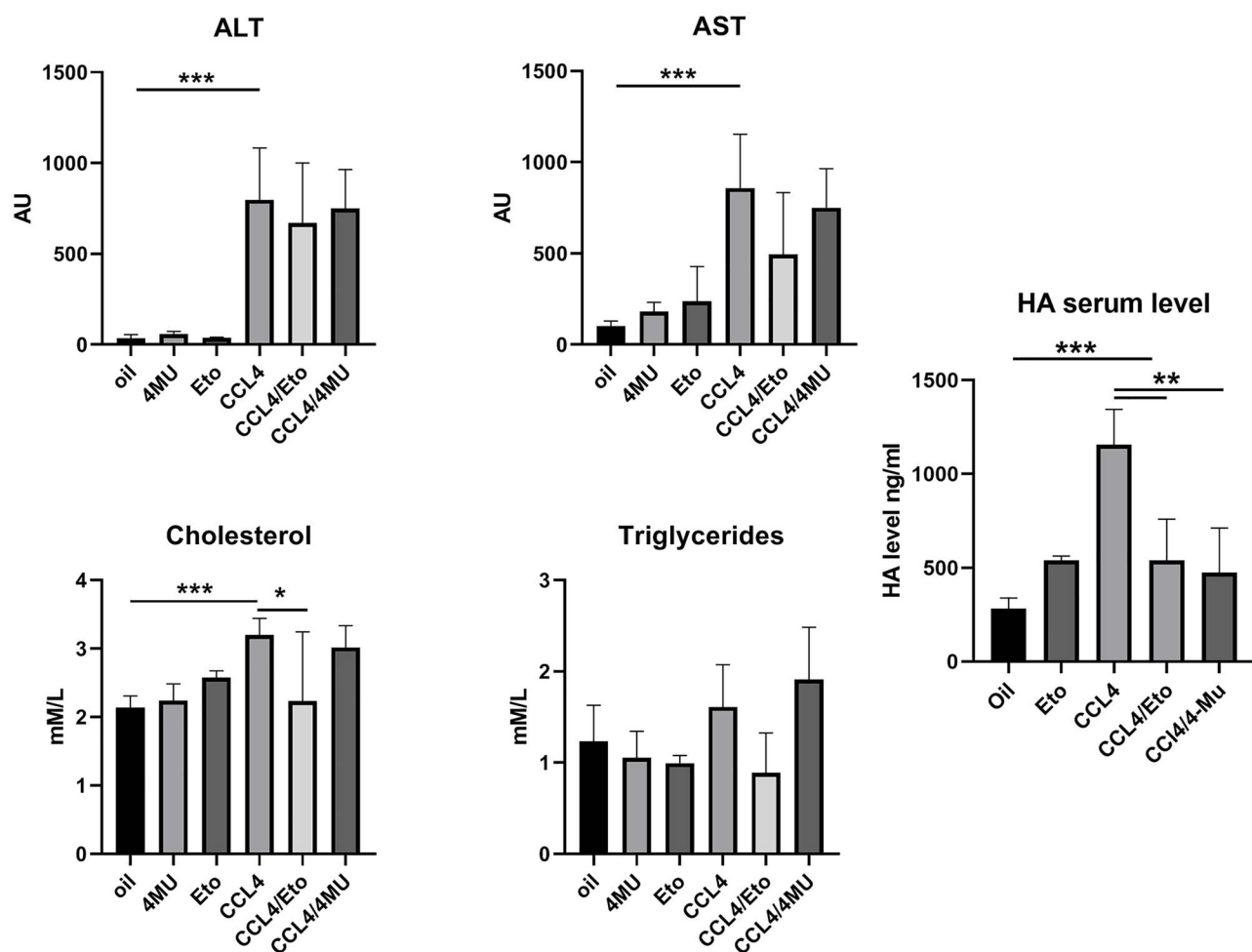


**Fig. 6.** Levels of the markers of liver cells injury ALT and AST, HA concentration and lipids concentrations in the plasma of mice with CCl<sub>4</sub> induced fibrosis treated with 4MU and etoxazole. \*\*\*— $P < 0.001$  one-way ANOVA,  $n = 8$ , data present as mean  $\pm$  SD. This figure is available in black and white in print and in color at *Glycobiology* online.

point mutation I1056F/M corresponding to I1017F in *T. urticae* (Douris et al. 2016). Of note, the invariant Ile in the 5TMS domain in wild-type *Drosophila* strains is also followed by Pro, which is separated from the WGTR signature by 20 amino acids.

In mammalian HAS1, HAS2 and HAS3, the  $\alpha$  helix domain MD5 (marked red in Figure 9.) correspond to 5TMS of CHS. This domain is modelled as an amphipathic helix, which does not cross the plasma membrane and hence would determine the C terminus of all HAS members to be oriented towards the cytoplasm (Weigel et al. 1997). It was confirmed by our 3D structure analysis using I-TASSER protein structure and function prediction server (Yang and Zhang 2015). Interestingly, it is now believed that the corresponding  $\alpha$ -helix in the 5TMS chitin synthase domain also does not pass through the membrane and serves as a pore organizer with a WGTR signature on the cytoplasm side (Gohlke et al. 2017). With the nonpassing topology of the fifth  $\alpha$ -helix, the deletion of four residues in human and mouse HAS (Figure 9D) becomes possible because the helix does not have to cross the membrane and thus, does not have to have the constant length: this deletion corresponds to the removal of one helical turn. The nonpassing topology of the fifth  $\alpha$ -helix is also better consistent with helix-breaking proline residue in the middle of the helix.

MD5 domain is adjacent to the Bx7B motif present in both mammalian and bacterial Streptococcus HAS (SeHAS; Figure 9C). Studies of several SeHAS mutants with point substitution of amino acids in the Bx7B motif suggested that it is involved in size regulation and HA polymer translocation across the membrane. (Baggenstoss et al. 2017).

All of the above allows us to suggest that reduced production of HA by NIH3T3 cells in the presence of etoxazole, triflumuron and buprofezin can be explained by their direct interaction with the region immediately following the MD5 amphiphilic cytoplasm domain of HAS. It will be interesting to investigate the possibility of reducing the inhibitory effect of etoxazole and BPU compounds by substituting Leu-447 residue. These structural and genetic data support the hypothesis that etoxazole inhibits both chitin synthase and hyaluronan synthase by direct interaction with the 5TMS (MD5) domain, a part of the pore through which chitin or HA are extruded.

Recently it was shown that etoxazole inhibits cardiovascular development in zebrafish embryos (Park et al. 2019). The phenotype comprised heart underdevelopment, pericardial oedema and abnormalities of dorsoventral specification. This phenotype resembled in milder version morphans produced by HAS2 morpholino

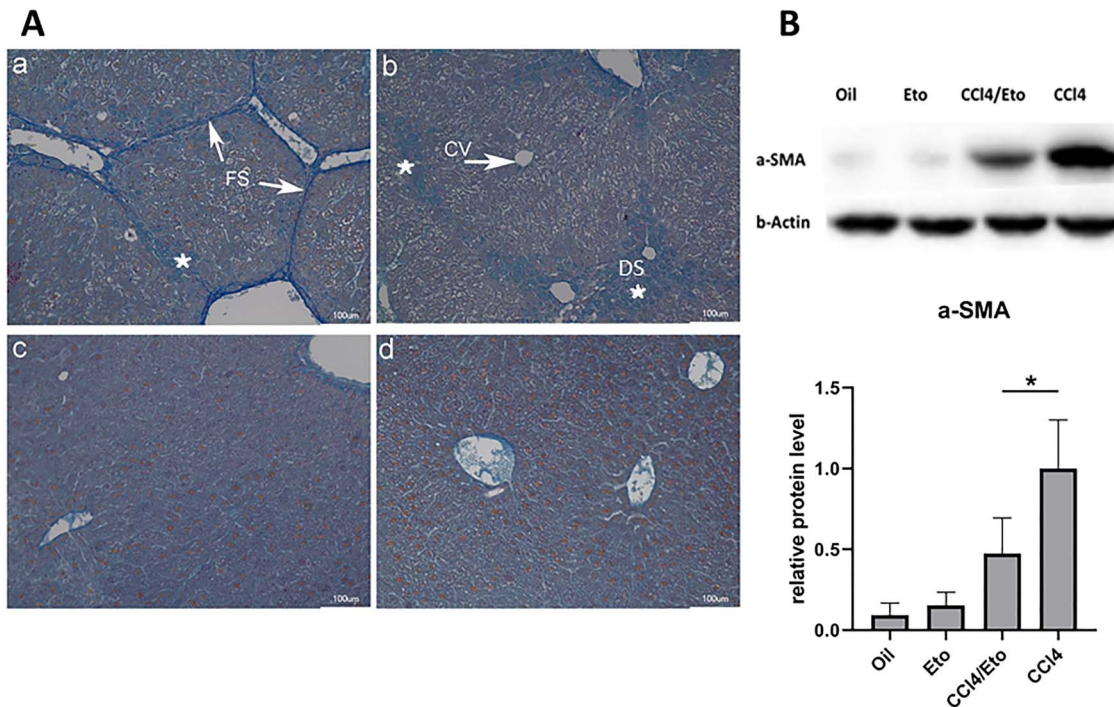


**Fig. 7.** Etoxazole reduces liver fibrosis and alpha-SMA expression in CCl<sub>4</sub> liver induced fibrosis. **(A)** Mallory trichrome staining of the liver. Experimental groups: **(a)** mice treated with CCl<sub>4</sub> alone, **(b)** CCl<sub>4</sub> + Eto, **(c)** oil, **(d)** etoxazole alone. FS—a fibrous scar, DS—particulate collagen staining, CV—central vein, \*—aniline blue-stained cells. Scale bar—100  $\mu$ m. **(B)** Quantitative western blot analysis of  $\alpha$ SMA in liver homogenate \*  $P < 0.05$ ,  $n = 5$ ,  $t$ -test. This figure is available in black and white in print and in color at *Glycobiology* online.

injected in zebrafish fertilized egg (Bakkers et al. 2004). Developmental abnormalities resulting from HAS2 loss of function in vertebrates (zebrafish, mouse and *Xenopus*) can be explained by an aberrant endothelial-to-mesenchymal transition which results in failure to form endocardial cushions and a loss of their cellularization (Lagendijk et al. 2013). Interestingly, these phenotypes similar to those observed in etoxazole treated zebrafish larva (Park et al. 2019) were also described in zebrafish valveless Jekyll mutant (Walsh and Stainier 2001) with the loss of function of UDP-glucose dehydrogenase (UGDH). This enzyme synthesizes GlcA, the main precursor of HA. UGDH is expressed explicitly in ECs of mouse embryos and is required for efficient HA synthesis in zebrafish. Recently natural polymorphic variants of the UGDH gene with decreased enzyme stability were identified in patients with congenital cardiac valve-related defects (Hyde et al. 2012). Of note, knockout of Has2 in mice was embryonal lethal due to cardiac valve formation, which cannot be compensated for by the other Has enzymes (Camenisch et al. 2000). These embryological and genetic data corroborate our hypothesis that etoxazole interferes with HA production, possibly by direct interaction with HAS2 protein.

In conclusion, our experimental data on inhibition of HA secretion in cell culture together with the analysis of domain homology between HAS and chitin synthase points towards chitin synthesis inhibitors, particularly etoxazole, buprofezin and triflumuron as compounds that may directly interact with HAS2. Direct interaction of etoxazole, buprofezin and triflumuron with the pore organizing domain of chitin synthase (Douris et al. 2016) indicates the possibility of similar direct interactions of these compounds with hyaluronan synthase, which will be the subject of further investigations. Our research will help design new clinically relevant specific inhibitors of excessive hyaluronan secretion, a vital disease marker and

pathological phenomena in fibrosis, inflammatory disorders and cancer metastasis.

## Materials and methods

### Chemicals and compounds

Buprofezin (672928, HPC Standards GmbH, Germany), Etoxazole (675816, HPC Standards GmbH, Germany), Lufenuron (673891, HPC Standards GmbH, Germany), Triflumuron (675080, HPC Standards GmbH, Germany), Difebenzuron (674699, HPC Standards GmbH, Germany), Nikkomycin Z from *Streptomyces tendae* (N8028, Sigma-Aldrich, St. Louis, MO, USA), 4-Methylubelliferone (M1381, Sigma-Aldrich, St. Louis, MO, USA), 3-Hydroxycoumarin (642673, Sigma-Aldrich, St. Louis, MO, USA; compound I) and 7-Methoxy-4-methylcoumarin (246131, Sigma-Aldrich, St. Louis, MO, USA; compound II).

Analogues of 4-MU were synthesized in the laboratory Taras Shevchenko National University of Kyiv, Faculty of chemistry, using the protocol described previously (Moskvina and Khilya 2008; Moskvina et al. 2014; Glibov et al. 2018). The detailed synthesis is described in Supplementary. All substances were dissolved in DMSO (A1584, AppliChem GmbH, Germany).

### Cell culture

NIH3T3 (ATCC<sup>®</sup> CRL-1658<sup>™</sup>) cell line was cultured in DMEM (C435p, PanEco, Russia) +10% FBS (A3160501, Gibco, Thermo Fisher, Waltham, MA, USA) and passaged three times per week.

### Doubling time calculation

For doubling time calculation, cells were seeded in a 96-well plate,  $2 \times 10^4$  cell per well and incubated with inhibitors added as DMSO

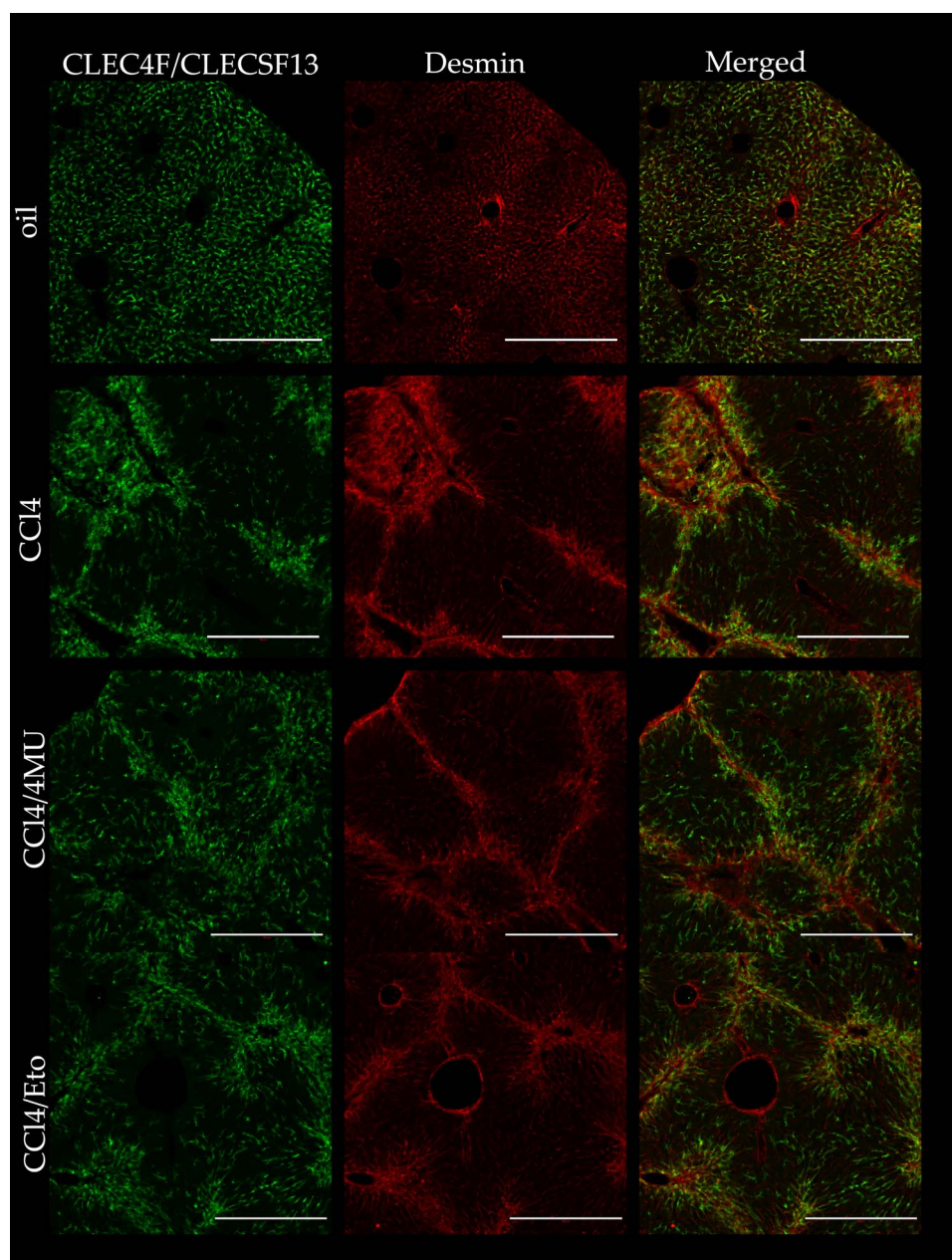


**Fig. 8.** Mutual localization of activated Hepatic stellate cells and Kupffer cells in CCl<sub>4</sub> fibrotic livers of mice treated with 4MU and etoxazole. Sections were stained with abs to desmin (marker for HSCs) and CLEC4F/CLECSF13 (a marker for Kupffer Cell). Scale bar—500  $\mu$ m. The image data were used to derive Manders colocalization coefficients (MCC) for KCs and HSCs cells (Table II). This figure is available in black and white in print and in color at *Glycobiology* online.

solutions at a 1:100 volume ratio. After 72 h of incubation, cells were fixed with 4% PFA and stained with 1  $\mu$ g/mL DAPI (D9542, Merck KGaA, Germany) in PBS for 10 min. After washing, the plate was imaged at Leica DMI6000 fluorescent microscope (Leica, Germany), and the cell number in each well was measured by CellProfiler software (<https://cellprofiler.org>). Doubling time was calculated using the formula:

$$N(t) = N(0)2^{t/dt}$$

$N(t)$ —the number of cells at the end of the experiment.

$N(0)$ —the number of cells at the start of the experiment.

$dt$ —doubling time, hours.

$t$ —time in hours.

All experiments for doubling time calculation of each compound were performed in three independent repeats, each containing three individual cell culture wells.

#### MTT assay

MTT (Thiazolyl Blue Tetrazolium Bromide) was from PanEco (Q105, Russia). MTT was dissolved in PBS to a final concentration 5 mg/mL and filtered through 0.22- $\mu$ m filter. 10  $\mu$ L of MTT solution was added to 100  $\mu$ L of cell culture medium and incubated for 3 h at 37°C, 5% of CO<sub>2</sub>. After incubation, cell plates were centrifuged at 1500 rpm for 5 min. Media were carefully removed, and 100  $\mu$ L of pure DMSO was added into each well. The absorbance of the resulting solution was measured at 570 nm by a multi-plate reader.

**Table II.** Colocalization of HSCs and Kupffer cells based on Manders coefficient

Group	MCC macrophages	MCC HSCs
Oil	0.15 ± 0.03	0.06 ± 0.008
CCl4	0.30 ± 0.07 **	0.27 ± 0.07 ***
CCl4/4MU	0.13 ± 0.02 ##	0.13 ± 0.03 ##
CCl4/Eto	0.14 ± 0.02 ##	0.15 ± 0.02 ##

\*\*— $P < 0.01$  comparing to oil. \*\*\*— $P < 0.001$  comparing to oil. ## $P < 0.01$  comparing to CCl<sub>4</sub>. Data present as mean ± SD,  $n = 3$ .

### Inhibitory assay of hyaluronan secreted in NIH3T3 cell culture media

For the experiment, cells were seeded in 96-well plates in density  $2 \times 10^4$  cells per well. On the next day, the medium was changed for a fresh one.

Inhibitors were dissolved in DMSO at 1-M concentration. Immediately before the experiments, 0.1-M solution in 10% DMSO/D-MEM was prepared and subjected to serial dilutions in DMEM. Aliquots of diluted inhibitors were added to the cell culture media at a 1:100 ratio so that the final DMSO concentration was not exceeded 0.1% v/v. Cells were incubated with and without inhibitors for 72 h; after that, 100  $\mu$ L of media were collected and froze at  $-20^\circ\text{C}$  for future analysis. As a control, we used 0.1% DMSO alone, which showed no effect on HA deposition, cell viability or doubling time.

The remaining cells were fixed in 4% PFA in PBS pH 7.4 and stained with 2  $\mu$ g/mL DAPI (D9542, Merck KGaA) for 10 min in PBS. After a brief wash, samples were imaged at Leica DMI6000 (Leica,

Germany) fluorescent microscope, equipped with HCX PL Fluotar  $10\times/0.30$  objective (15506505, Leica), excitation wavelength 385 nm and A filter cube (BP 340–380, DM 400, LP 425, Leica, Germany). The number of cells in each well was measured by CellProfiler software (<https://cellprofiler.org>).

On the day of analysis of cell culture, media samples were defrosted and diluted 1:10 with PBS. Hyaluronan concentration was detected using DuoSet Hyaluronan kit (DY3614, R&D System) according to manufacture recommendation. The HA concentration was calculated from calibration curves obtained with HA standard solutions and normalized to the number of cells in the corresponding well.

All cell culture experiments were repeated three times. The IC<sub>50</sub> was calculated using nonlinear regression analysis by GraphPad Prism 7.0 software.

### Microscopic evaluation of HA associated with NIH3T3 cells

Cells were seeded in 8-well chamber slides (Ibidi, 80827, Germany) in concentration  $2 \times 10^4$  cells per well. The next day after seeding, culture media were changed to the fresh ones containing 10  $\mu$ M of different inhibitors. After 3 days of incubation, cells were fixed in 10% buffered formalin (Biovitrum, Russia) for 10 min and washed three times with PBS. Testicular hyaluronidase (H3884, Sigma-Aldrich, St. Louis, MO, USA) digestion (1 mg/mL, 30 min,  $+37^\circ\text{C}$ ) of cells not treated with inhibitors were used as the negative control. Nonspecific binding was blocked by Avidin-Biotin blocking kit (ab64212, Abcam, UK) according to manufacture recommendation and incubated with biotinylated HABP probe (385911, Merck, USA) overnight

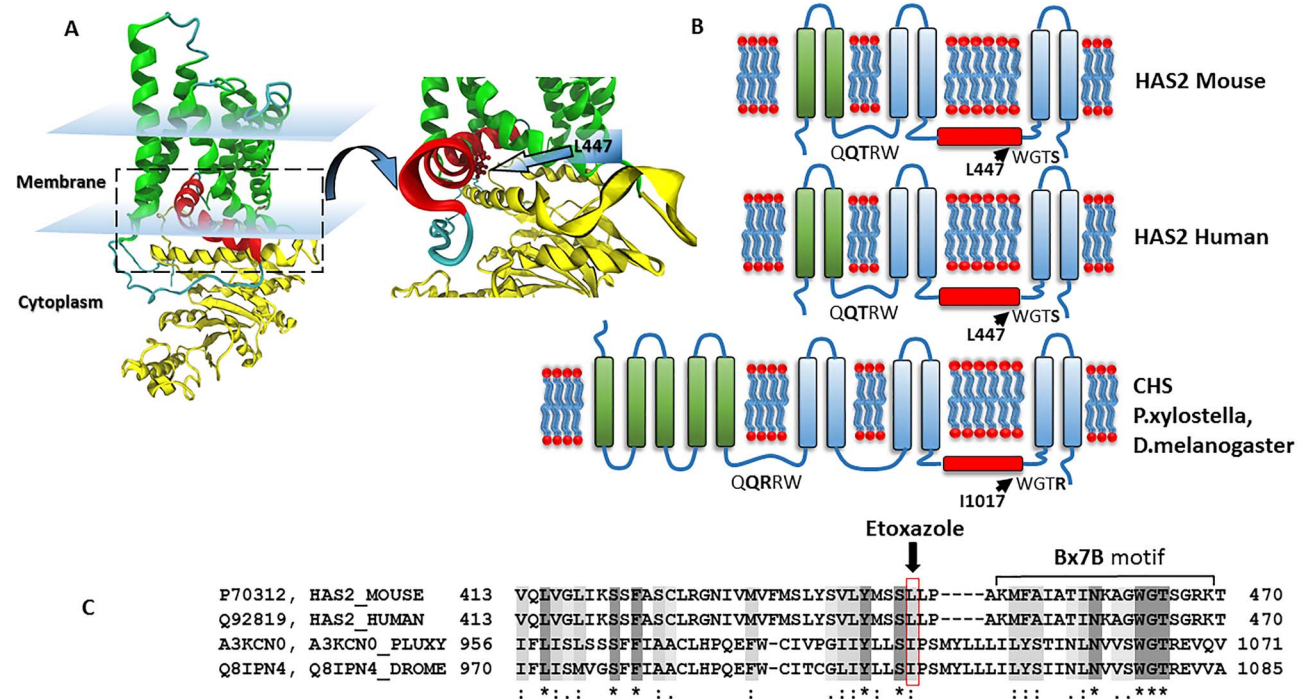


**Fig. 9.** Comparison of the domain organization of HAS (mouse and human) and chitin synthase (*P. xylostella*, *D. melanogaster*). (A) Predicted 3D structure of HAS2. (B) Schematic comparison of HAS2 and chitin synthases—N-terminal transmembrane domains are colored in green, C-terminal transmembrane domains are blue. The catalytic center for HAS and CHS contained Q\*\*RW conservative motif. The Bx7B motif is indicated by a horizontal bracket. Both  $\alpha$ -helix MD5 domain of HAS2 and 5TMS domain of chitin synthase marked in red. (C) Alignment of the amino acid sequences of HAS and CHS showed a conserved WGT(S/R) motif. Leu-447 for HAS and Ile-1017 for CHS essential for interaction with etoxazole marked with the arrow. (\*)—conserved residue, (:)—scoring  $> 0.5$ , (.)—scoring  $\leq 0.5$ . This figure is available in black and white in print and in color at *Glycobiology* online.

+4°C. After careful washing with PBS, Streptavidin Alexa Fluor 488 conjugate (S32354, 1:500, Thermo Fisher, USA), Hoechst 33342 (1 µg/mL, H3570, Thermo Fisher, USA) and Phalloidine Alexa Fluor 633 (A22284, 1:500, Thermo Fisher, USA) were added in PBS and incubated for 1 h at RT. Washed samples were mounted in ProLong Glass Antifade (P36982, Thermo Fisher, USA) and imaged by Carl Zeiss LSM880 confocal microscope (Carl Zeiss, Germany) equipped with Plan-Apochromat 40×/1.4 Oil DIC M27 objective. Mosaic frame 5 × 5 field of view was taken from each sample in multitrack mode; the number of biological repeats for each tested compound was three wells. HA positive area and total cell area were measured in each field of view for each sample by ImageJ v.1.52 (NIH, USA) software.

### Animal experiments

All regulated animal procedures were approved following the Ethics Committees for Animal Research of the Koltzov Institute of Developmental Biology under Laboratory Practice Regulations in the Russian Federation. Animal experiments were consistent with the recommendations of ARRIVE (Kilkenny et al. 2010).

8-week old female Balb/c mice (weight 18.22 g) were obtained from “Scientific Center for Biomedical Technologies” of the Federal Medical and Biological Agency, Moscow, Russia. They were maintained in the animal facility of controlled light/dark cycle and relative humidity 55–65%. All groups were provided with free access to the standard diet and water. Mice acclimatization to the conditions lasted 2–3 days before the experiments start. Liver damage was induced by intraperitoneal administration of CCl<sub>4</sub> in olive oil in dosage 0,5 µL/g mouse body weight. Etoazole and 4MU were prepared by mixing with 0.5% methylcellulose, given per os by gavage at a 600 mg/kg daily concentration. Control mice were gavaged in the same way with 0.5% methylcellulose slurry. The administration of 4MU and etoazole were started 2 days before the first injection and lasted for 2 weeks. The experiment consisted of four groups of animals ( $n = 8$ ). At the end of 2 weeks of treatment, animals were terminally anaesthetized with 5% isoflurane and euthanized by fast exsanguination followed by cervical dislocation. Samples were collected for blood analysis and histological examination. Separate groups of animals were used for immunohistochemical examinations and confocal microscopy.

### Blood serum collection and ALT/AST, cholesterol and triglycerides measurement

Whole blood was sampled from the left ventricle after culling the animal. Blood samples were left for coagulation for 1 h on ice. The serum was purified by centrifugation for 40 min at 3000 rpm and frozen at –20°C for storage. The ALT/AST level was measured by the commercial biomedical analytical laboratory ChanceBio, Moscow, Russia.

### Histology

Freshly isolated liver samples were fixed Davidson’s fixative for 24 h. After an extensive wash in H<sub>2</sub>O, samples were dehydrated in isopropanol solutions with a rising concentration from 70 to 100% and then embedded in Histomix (Biovitrum, Russia) +56°C. Embedded tissue samples were sectioned by microtome at 5-µm slices and mounted onto SuperFrost glass slides. For Mallory staining, we used commercially-available kits (Biovitrum, Russia). The photos of histological specimens were taken with microscope Keyence BZ9000 BioRevo (Yokogawa Electric Corporation, Japan).

### Immunochemistry and confocal microscopy

For the confocal microscopy study, we used separate groups of mice ( $n = 4–8$ ). Mice were terminally anaesthetized by 5% isoflurane inhalation and perfused through their left ventricle with PBS, followed by 10% buffered formalin (Biovitrum, Russia) for 20 min. Liver lobes were cut off and additionally fixed in 10% buffered formalin for 2 h at RT. Then samples were washed by PBS and cut for 50-µm slices by vibratome sectioning. Vibratome sections were permeabilized in PBS-0.2% Triton X-100 for 1 h, followed by incubation with primary antibody for 2 days at +4°C. After several washes with PBS-0.2% Triton X-100, sections were incubated with appropriate secondary antibody for one night. Washed sections were mounted in TDE-mounting media and analyzed by laser scanning confocal microscopy. Images were taken by a Carl Zeiss LSM880 confocal microscope (Carl Zeiss, Germany) equipped with 25× oil immersion objective (LCI “Plan-Neofluar” 25×/0.8 Imm Corr Ph2 M27, Carl Zeiss), 488 and 640-nm wavelength diode-lasers were used for fluorochrome excitation. Mosaic frame Z-stack, 4 × 4 fields of view in size with 10% overlap, were scanned on each sample with 2-µm optical section step. Each channel was scanned as a separate track to avoid overlapping of emission signals (sequential scanning). The following primary antibodies were used: anti-desmin (ab15200, Abcam, USA) 1:300, anti-CLEC4F\CLECSF13 (AF2784, R&D Systems, USA) 1:300.

Secondary antibodies were: Donkey anti-rabbit Alexa Fluor 488 (A-21206, 1:1000, Invitrogen, USA); Donkey anti-Goat Alexa Fluor® 647 (A-32849, 1:1000, Invitrogen, USA).

### Topological analysis

For estimation of proximity between macrophages and HSCs, sections were stained for corresponding markers CLEC4F\CLECSF13 and Desmin. Manders’ colocalization coefficient (MCC) was calculated using Imaris 7.4.2 (Bitplane, Switzerland). For paired markers, R and G, two different values of MCC derived, M1, the fraction of R in compartments containing G and M2, the fraction of G in compartments containing R. M1 and M2 were calculated as:

$$M1 = \frac{\sum_i R_i \text{ coloc}}{\sum_i R_i}$$

$$M2 = \frac{\sum_i G_i \text{ coloc}}{\sum_i G_i}$$

### Quantitative real-time polymerase chain reaction (qPCR) analysis

Total RNA from fresh tissue samples was isolated by TRI reagent (Sigma-Aldrich) according to the manufacturer’s protocol. The total RNA concentration and quality were determined using the NanoDrop 2000 spectrophotometer (Thermo Fisher Scientific, USA) and electrophoresis. To eliminate genomic DNA contamination from RNA samples DNA-free™ DNase Treatment and Removal Reagents (Ambion, Thermo Fisher Scientific, USA) were used. 2 µg total RNA was used for cDNA synthesis by Mint-2 (Evrogen, Moscow, Russia) cDNA synthesis kit and random primers according to the manufacturer’s protocol. Evaluation of mRNA Expression Levels of target genes was measured using qPCR mix-HS HighROX SYBR (Evrogen, Moscow, Russia) and Applied Biosystems StepONE Plus Real-Time PCR System (Thermo Fisher Scientific, USA). All data were presented as mean ± SD of three independent technical replicates and normalized to the level of glyceraldehyde 3-phosphate dehydrogenase

**Table III.** Oligonucleotide sequence of primers used for Q-PCR

Gene	Direction	Sequence
moHas2	Forward	5'-AGGTCGGTGTGAACGGATTTG-3'
	Reverse	5'-GAGAGCCTCAGGATAACT-3'
moHas3	Forward	5'-GACTGTGCCTGAGATAATGAG-3'
	Reverse	5'-ATTCCTTACTTCTGGTGAAGTTC-3'
moHyal1	Forward	5'-AACAAGTACCAAGGAATCAT-3'
	Reverse	5'-GAGAGCCTCAGGATAACT-3'
moHyal2	Forward	5'-CGCTTCAAGTATGGAGAC-3'
	Reverse	5'-GGTCCAAGTCAATACTG-3'
GAPDH	Forward	5'-AGGTCGGTGTGAACGGATTTG-3'
	Reverse	5'-TGTAGACCATGTAGTTGAGGTCA-3'

(GAPDH) mRNA. Statistical significance between different groups was determined using one-way analysis of variance (ANOVA). The list of primers for quantitative reverse transcriptase-polymerase chain reaction can be found in Table III:

### Western-blot

Tissue samples (50 mg) were solubilized in Ripa Buffer (89900, Thermo Fisher) with the addition of EASYpack protease inhibitors (5892970001, Roche, Switzerland). Protein concentration in supernatants after 14,000 rpm centrifugation was determined using the BCA method. 25 µg of protein were separated on 8% SDS-PAGE with subsequent blotting on a nitrocellulose membrane (BIO-RAD, USA) using Trans-Blot<sup>®</sup> Turbo<sup>™</sup> Transfer System (Bio-Rad, USA) with subsequent immersion in 5% skimmed milk in TBST buffer. Primary ab: anti- $\alpha$ SMA (ab5694, Abcam, UK); anti-beta Actin (ab16039, Abcam, UK). Secondary ab: 1:10,000-anti-Mouse IgG (H + L) secondary antibody (115-005-003, Jackson ImmunoResearch, USA), anti-Rabbit IgG (H + L) secondary antibody (111-035-144, Jackson ImmunoResearch, USA). Signal was revealed by the ECL method following the HRP reaction.

### Sequence alignment

Protein sequences were obtained from the UniProt (<https://www.uniprot.org/>; UniProt 2019) and NCBI (<https://www.ncbi.nlm.nih.gov/>) (2016). The UniProt database determined the position and the domain type of the studied proteins. Protein multiple sequence alignment was constructed by the MUSCLE algorithm (Edgar 2004). The following protein sequences were used for analysis: hyaluronan synthase 2 from *Mus musculus* (UniProt: P70312, HAS2\_MOUSE), hyaluronan synthase 2 from *Homo sapiens* (UniProt: Q92819, HAS2\_HUMAN), CHS 1 from *P. xylostella* (UniProt: A3KCN0, A3KCN0\_PLUXY) and Krotzkopf verkehrt from *D. melanogaster* (UniProt: Q8IPN4, Q8IPN4\_DROME).

### 3D structure prediction

The primary amino acid structure of mouse HAS2 was submitted to protein structure and function prediction server I-TASSER (<https://zhanglab.ccmb.med.umich.edu/I-TASSER/>) (Yang and Zhang 2015). Visualization was achieved with VMD version 1.9.3 (Humphrey et al. 1996).

### Statistical analysis

Data are presented as mean value  $\pm$  SD. Statistical analyses were performed using a one-way ANOVA and Kolmogorov–Smirnov test for rank as appropriate using Graph Pad Prism 8 software. Differences were considered significant at values of  $P < 0.05$ . All cell culture experiments were repeated 3 times. The IC<sub>50</sub> was calculated using nonlinear regression analysis by GraphPad Prism 7.0 software.

### Abbreviations

4MU, 4-methylumbelliferone; ALT, alanine aminotransferase; AST, aspartate aminotransferase; CHS, chitin synthases; DMSO, dimethyl sulfoxide; HA, hyaluronic acid; HABP, hyaluronan binding protein; HAS, hyaluronan synthases; HSC, hepatic stellate cells; KCs, Kupffer Cells

### Supplementary data

Supplementary data are available at *Glycobiology* online.

### Acknowledgements

The research was done using equipment of the Core Centrum of the Institute of Developmental Biology RAS.

### Funding

The work was supported by Russian Foundation for Basic Research (grant no. 19-29-04123); and the Government program of basic research in Koltzov Institute of Developmental Biology of the Russian Academy of Sciences (grant no. 0088-2021-0017, 2021).

### Conflicts of interest statement

The authors state no conflict of interest.

### References

- Agarwal G, Kv K, Prasad SB, Bhaduri A, Jayaraman G. 2019. Biosynthesis of hyaluronic acid polymer: Dissecting the role of sub structural elements of hyaluronan synthase. *Sci Rep.* 9(1):12510.
- Andreichenko IN, Tsitrina AA, Fokin AV, Gabdulkhakova AI, Maltsev DI, Perelman GS, Bulgakova EV, Kulikov AM, Mikaelyan AS, Kotelevtsev YV. 2019. 4-methylumbelliferone prevents liver fibrosis by affecting hyaluronan deposition, FSTL1 expression and cell localization. *Int J Mol Sci.* 20(24):6301.
- Baggenstoss BA, Harris EN, Washburn JL, Medina AP, Nguyen L, Weigel PH. 2017. Hyaluronan synthase control of synthesis rate and hyaluronan product size are independent functions differentially affected by mutations in a conserved tandem B-X7-B motif. *Glycobiology.* 27(2):154–164.
- Bakkers J, Kramer C, Pothof J, Quaedvlieg NEM, Spaijk HP, Hammerschmidt M. 2004. Has2 is required upstream of Rac1 to govern dorsal migration of lateral cells during zebrafish gastrulation. *Development.* 131(3):525–537.
- Camenisch TD, Spicer AP, Brehm-Gibson T, Biesterfeldt J, Augustine ML, Calabro A, Kubalak S, Klewer SE, McDonald JA. 2000. Disruption of hyaluronan synthase-2 abrogates normal cardiac morphogenesis and hyaluronan-mediated transformation of epithelium to mesenchyme. *J Clin Invest.* 106(3):349–360.
- Cohen E. 2001. Chitin synthesis and inhibition: A revisit. *Pest Manag Sci.* 57(10):946–950.
- Cordes FS, Bright JN, Sansom MSP. 2002. Proline-induced distortions of transmembrane helices. *J Mol Biol.* 323(5):951–960.

- NCBI Resource Coordinators. 2016. Database resources of the National Center for biotechnology information. *Nucleic Acids Res.* 44(Database issue):D7–D19.
- DeAngelis PL, Yang N, Weigel PH. 1994. The streptococcus pyogenes hyaluronan synthase: Sequence comparison and conservation among various group a strains. *Biochem Biophys Res Commun.* 199(1):1–10.
- Demaeght P, Osborne EJ, Odman-Naresh J, Grbić M, Nauen R, Merzendorfer H, Clark RM, Van Leeuwen T. 2014. High resolution genetic mapping uncovers chitin synthase-1 as the target-site of the structurally diverse mite growth inhibitors clofentezine, hexythiazox and etoxazole in *Tetranychus urticae*. *Insect Biochem Mol Biol.* 51:52–61.
- Douris V, Steinbach D, Panteleri R, Livadaras I, Pickett JA, Van Leeuwen T, Nauen R, Vontas J. 2016. Resistance mutation conserved between insects and mites unravels the benzoylurea insecticide mode of action on chitin biosynthesis. *Proc Natl Acad Sci U S A.* 113(51):14692–14697.
- Edgar RC. 2004. MUSCLE: Multiple sequence alignment with high accuracy and high throughput. *Nucleic Acids Res.* 32(5):1792–1797.
- Geremia RA, Mergaert P, Geelen D, Van Montagu M, Holsters M. 1994. The NodC protein of *Azorhizobium caulinodans* is an N-acetylglucosaminyltransferase. *Proc Natl Acad Sci U S A.* 91(7):2669–2673.
- Glibov EK, Moskvina VS, Khilya VP. 2018. Coumarins mannich bases in acylation reactions. *Ukr Chem J.* 84(2):93–101.
- Gohlke S, Muthukrishnan S, Merzendorfer H. 2017. In vitro and in vivo studies on the structural organization of Chs3 from *Saccharomyces cerevisiae*. *Int J Mol Sci.* 18(4):702.
- Grandoch M, Flögel U, Virtue S, Maier JK, Jelenik T, Kohlmorgen C, Feldmann K, Ostendorf Y, Castañeda TR, Zhou Z, et al. 2019. 4-Methylumbelliferone improves the thermogenic capacity of brown adipose tissue. *Nat Metab.* 1(5):546–559.
- Guillot A, Buch C, Jourdan T. 2020. Kupffer cell and monocyte-derived macrophage identification by immunofluorescence on formalin-fixed, paraffin-embedded (FFPE) mouse liver sections. *Methods Mol Biol.* 2164:45–53.
- Humphrey W, Dalke A, Schulten K. 1996. VMD: Visual molecular dynamics. *J Mol Graph.* 14(1):33–38 27–28.
- Hyde AS, Farmer EL, Easley KE, van Lammeren K, Christoffels VM, Barycki JJ, Bakkers J, Simpson MA. 2012. UDP-glucose dehydrogenase polymorphisms from patients with congenital heart valve defects disrupt enzyme stability and quaternary assembly. *J Biol Chem.* 287(39):32708–32716.
- Kakizaki I, Kojima K, Takagaki K, Endo M, Kannagi R, Ito M, Maruo Y, Sato H, Yasuda T, Mita S, et al. 2004. A novel mechanism for the inhibition of hyaluronan biosynthesis by 4-methylumbelliferone. *J Biol Chem.* 279(32):33281–33289.
- Kakizaki I, Takagaki K, Endo Y, Kudo D, Ikeya H, Miyoshi T, Baggenstoss BA, Tlapak-Simmons VL, Kumari K, Nakane A, et al. 2002. Inhibition of hyaluronan synthesis in *Streptococcus equi* FM100 by 4-methylumbelliferone. *Eur J Biochem.* 269(20):5066–5075.
- Kilkenny C, Browne WJ, Cuthill IC, Emerson M, Altman DG. 2010. Improving bioscience research reporting: The ARRIVE guidelines for reporting animal research. *PLOS Biology.* 8(6):e1000412.
- Kudo D, Suto A, Hakamada K. 2017. The development of a novel therapeutic strategy to target hyaluronan in the extracellular matrix of pancreatic ductal adenocarcinoma. *Int J Mol Sci.* 18(3):600.
- Kuipers HF, Nagy N, Ruppert SM, Sunkari VG, Marshall PL, Gebe JA, Ishak HD, Keswani SG, Bollyky J, Frymoyer AR, et al. 2016. The pharmacokinetics and dosing of oral 4-methylumbelliferone for inhibition of hyaluronan synthesis in mice. *Clin Exp Immunol.* 185(3):372–381.
- Kultti A, Pasonen-Seppänen S, Jauhainen M, Rilla KJ, Kärnä R, Pyöriä E, Tammi RH, Tammi MI. 2009. 4-Methylumbelliferone inhibits hyaluronan synthesis by depletion of cellular UDP-glucuronic acid and downregulation of hyaluronan synthase 2 and 3. *Exp Cell Res.* 315(11):1914–1923.
- Legendijk AK, Szabó A, Merks RMH, Bakkers J. 2013. Hyaluronan: A critical regulator of endothelial-to-mesenchymal transition during cardiac valve formation. *Trends Cardiovasc Med.* 23(5):135–142.
- Mason RM, Lineham JD, Phillipson MA, Black CM. 1984. Selective inhibition of proteoglycan and hyaluronate synthesis in chondrocyte cultures by cyclofenil diphenol, a non-steroidal weak oestrogen. *Biochem J.* 223(2):401–412.
- Merzendorfer H. 2006. Insect chitin synthases: A review. *J Comp Physiol B, Biochem Syst Environ Physiol.* 176(1):1–15.
- Merzendorfer H, Zimoch L. 2003. Chitin metabolism in insects: Structure, function and regulation of chitin synthases and chitinases. *J Exp Biol.* 206(Pt 24):4393–4412.
- Meyer MF, Kreil G. 1996. Cells expressing the DG42 gene from early *Xenopus* embryos synthesize hyaluronan. *Proc Natl Acad Sci U S A.* 93(10):4543–4547.
- Mian N. 1986. Analysis of cell-growth-phase-related variations in hyaluronate synthase activity of isolated plasma-membrane fractions of cultured human skin fibroblasts. *Biochem J.* 237(2):333–342.
- Morohashi H, Kon A, Nakai M, Yamaguchi M, Kakizaki I, Yoshihara S, Sasaki M, Takagaki K. 2006. Study of hyaluronan synthase inhibitor, 4-methylumbelliferone derivatives on human pancreatic cancer cell (KP1-NL). *Biochem Biophys Res Commun.* 345(4):1454–1459.
- Moskvina VS, Khilya VP. 2008. Synthesis of pyrano[2,3-f]chromen-2,8-diones and pyrano[3,2-g]chromen-2,8-diones based on o-hydroxyformyl(acyl)neoflavonoids. *Chem Natl Compd.* 44(1):16.
- Moskvina VS, Masich DY, Khilya VP, Khilya VP. 2014. Pyranoneoflavonoids: Synthesis and structure. *Dopov Nac akad nauk Ukr.* 12:122–127.
- Nagy N, Freudenberger T, Melchior-Becker A, Röck K, ter Braak M, Jastrow H, Kinzig M, Lucke S, Suvorova T, Kojda G, et al. 2010. Inhibition of hyaluronan synthesis accelerates murine atherosclerosis: Novel insights into the role of hyaluronan synthesis. *Circulation.* 122(22):2313–2322.
- Nagy N, Gurevich I, Kuipers HF, Ruppert SM, Marshall PL, Xie BJ, Sun W, Malkovskiy AV, Rajadas J, Grandoch M, et al. 2019. 4-Methylumbelliferone glucuronide contributes to hyaluronan synthesis inhibition. *J Biol Chem.* 294(19):7864–7877.
- Nagy N, Kuipers HF, Frymoyer AR, Ishak HD, Bollyky JB, Wight TN, Bollyky PL. 2015. 4-Methylumbelliferone treatment and hyaluronan inhibition as a therapeutic strategy in inflammation, autoimmunity, and cancer. *Front Immunol.* 6:123.
- Nakamura T, Funahashi M, Takagaki K, Munakata H, Tanaka K, Saito Y, Endo M. 1997. Effect of 4-methylumbelliferone on cell-free synthesis of hyaluronic acid. *Biochem Mol Biol Int.* 43(2):263–268.
- Nakamura T, Takagaki K, Shibata S, Tanaka K, Higuchi T, Endo M. 1995. Hyaluronin-acid-deficient extracellular matrix induced by addition of 4-methylumbelliferone to the medium of cultured human skin fibroblasts. *Biochem Biophys Res Commun.* 208(2):470–475.
- Niki T, Pekny M, Hellemans K, Bleser PD, Berg KV, Vaeyens F, Quartier E, Schuit F, Geerts A. 1999. Class VI intermediate filament protein nestin is induced during activation of rat hepatic stellate cells. *Hepatology.* 29(2):520–527.
- Park H, Lee J-Y, Park S, Song G, Lim W. 2019. Developmental toxicity and angiogenic defects of etoxazole exposed zebrafish (*Danio rerio*) larvae. *Aquat Toxicol.* 217:105324.
- Prehm P. 2005. Inhibitors of hyaluronan export prevent proteoglycan loss from osteoarthritic cartilage. *J Rheumatol.* 32(4):690–696.
- Prehm P. 2013. Curcumin analogue identified as hyaluronan export inhibitor by virtual docking to the ABC transporter MRP5. *Food Chem Toxicol.* 62:76–81.
- Prehm P, Schumacher U. 2004. Inhibition of hyaluronan export from human fibroblasts by inhibitors of multidrug resistance transporters. *Biochem Pharmacol.* 68(7):1401–1410.
- Puche JE, Saiman Y, Friedman SL. 2013. Hepatic stellate cells and liver fibrosis. *Compr Physiol.* 3(4):1473–1492.
- Pummill PE, Achyuthan AM, DeAngelis PL. 1998. Enzymological characterization of recombinant *Xenopus* DG42, a vertebrate hyaluronan synthase. *J Biol Chem.* 273(9):4976–4981.
- Rosa F, Sargent TD, Rebbert ML, Michaels GS, Jamrich M, Grunz H, Jonas E, Winkles JA, Dawid IB. 1988. Accumulation and decay of DG42 gene products follow a gradient pattern during *Xenopus* embryogenesis. *Dev Biol.* 129(1):114–123.
- Saito T, Tamura D, Nakamura T, Makita Y, Ariyama H, Komiyama K, Yoshihara T, Asano R. 2013. 4-Methylumbelliferone leads to growth

- arrest and apoptosis in canine mammary tumor cells. *Oncol Rep.* 29(1): 335–342.
- Sargent TD, Dawid IB. 1983. Differential gene expression in the gastrula of *Xenopus laevis*. *Science.* 222(4620):135–139.
- Sato N, Cheng X-B, Kohi S, Koga A, Hirata K. 2016. Targeting hyaluronan for the treatment of pancreatic ductal adenocarcinoma. *Acta Pharm Sin B.* 6(2):101–105.
- Saxena IM, Brown RM, Dandekar T. 2001. Structure–function characterization of cellulose synthase: Relationship to other glycosyltransferases. *Phytochemistry.* 57(7):1135–1148.
- Semino CE, Robbins PW. 1995. Synthesis of “nod”-like chitin oligosaccharides by the *Xenopus* developmental protein DG42. *Proc Natl Acad Sci U S A.* 92(8):3498–3501.
- Spicer AP, McDonald JA. 1998. Characterization and molecular evolution of a vertebrate hyaluronan synthase gene family. *J Biol Chem.* 273(4):1923–1932.
- Stern R. 2017. Go fly a chitin: The mystery of chitin and chitinases in vertebrate tissues. *Front Biosci.* 22(4):580–595.
- Sukowati CHC, Anfuso B, Fiore E, Ie SI, Raseni A, Vascotto F, Avellini C, Mazzolini G, Tiribelli C. 2019. Hyaluronic acid inhibition by 4-methylumbelliferone reduces the expression of cancer stem cells markers during hepatocarcinogenesis. *Sci Rep.* 9(1):1–11.
- Ueki N, Taguchi T, Takahashi M, Adachi M, Ohkawa T, Amuro Y, Hada T, Higashino K. 2000. Inhibition of hyaluronan synthesis by vesnarinone in cultured human myofibroblasts. *Biochim Biophys Acta (BBA) - Mol Cell Res.* 1495(2):160–167.
- UniProt Consortium. 2019. UniProt: A worldwide hub of protein knowledge. *Nucl Acids Res.* 47(D1):D506–D515.
- Van Leeuwen T, Demaeght P, Osborne EJ, Dermauw W, Gohlke S, Nauen R, Grbic M, Tirry L, Merzendorfer H, Clark RM. 2012. Population bulk segregant mapping uncovers resistance mutations and the mode of action of a chitin synthesis inhibitor in arthropods. *Proc Natl Acad Sci U S A.* 109(12):4407–4412.
- Varki A. 1996. Does DG42 synthesize hyaluronan or chitin?: A controversy about oligosaccharides in vertebrate development. *Proc Natl Acad Sci U S A.* 93(10):4523–4525.
- Vigetti D, Rizzi M, Viola M, Karousou E, Genasetti A, Clerici M, Bartolini B, Hascall VC, De Luca G, Passi A. 2009. The effects of 4-methylumbelliferone on hyaluronan synthesis, MMP2 activity, proliferation, and motility of human aortic smooth muscle cells. *Glycobiology.* 19(5):537–546.
- Walsh EC, Stainier DY. 2001. UDP-glucose dehydrogenase required for cardiac valve formation in zebrafish. *Science.* 293(5535):1670–1673.
- Weigel PH. 2015. Hyaluronan synthase: The mechanism of initiation at the reducing end and a pendulum model for polysaccharide translocation to the cell exterior. *Int J Cell Biol.* 2015:1–15.
- Weigel PH, Baggenstoss BA, Washburn JL. 2017. Hyaluronan synthase assembles hyaluronan on a [GlcNAc( $\beta$ 1,4)]n-GlcNAc( $\alpha$ 1 $\rightarrow$ )UDP primer and hyaluronan retains this residual chitin oligomer as a cap at the nonreducing end. *Glycobiology.* 27(6):536–554.
- Weigel PH, Hascall VC, Tammi M. 1997. Hyaluronan synthases. *J Biol Chem.* 272(22):13997–14000.
- Weigel PH, West CM, Zhao P, Wells L, Baggenstoss BA, Washburn JL. 2015. Hyaluronan synthase assembles chitin oligomers with -GlcNAc( $\alpha$ 1 $\rightarrow$ )UDP at the reducing end. *Glycobiology.* 25(6):632–643.
- Yang J, Zhang Y. 2015. Protein structure and function prediction using I-TASSER. *Curr Protoc Bioinf.* 52:5.8.1–5.8.15.
- Yang YM, Nouredin M, Liu C, Ohashi K, Kim SY, Ramnath D, Powell EE, Sweet MJ, Roh YS, Hsin I-F, et al. 2019. Hyaluronan synthase 2-mediated hyaluronan production mediates Notch1 activation and liver fibrosis. *Sci Transl Med.* 11(496):eaat9284.
- Yaron I, Shirazi I, Judovich R, Levartovsky D, Caspi D, Yaron M. 1999. Fluoxetine and amitriptyline inhibit nitric oxide, prostaglandin E2, and hyaluronic acid production in human synovial cells and synovial tissue cultures. *Arthritis Rheum.* 42(12):2561–2568.
- Zhang W, Watson CE, Liu C, Williams KJ, Werth VP. 2000. Glucocorticoids induce a near-total suppression of hyaluronan synthase mRNA in dermal fibroblasts and in osteoblasts: A molecular mechanism contributing to organ atrophy. *Biochem J.* 349(Pt 1):91–97.